ChemComm

Visualization of Inhomogeneous Current Distribution on ZrO_2-Coated $LiCoO_2$ Thin-Film Electrodes using Scanning Electrochemical Cell Microscopy

Journal:	*ChemComm*
Manuscript ID	CC-COM-11-2018-008916.R1
Article Type:	Communication

ChemComm

COMMUNICATION

Visualization of Inhomogeneous Current Distribution on ZrO_2-Coated $LiCoO_2$ Thin-Film Electrodes using Scanning Electrochemical Cell Microscopy

Received 00th January 20xx,
Accepted 00th January 20xx

DOI: 10.1039/x0xx00000x

www.rsc.org/

Hirotaka Inomata,[a] Yasufumi Takahashi,[*b, c] Daiko Takamatsu,[d] Akichika Kumatani,[a,e] Hiroki Ida, [a] Hitoshi Shiku,[f] Tomokazu Matsue,[*a, e]

Cathode surface coating with metal-oxide thin layers has been intensively studied to improve the cycle durability of lithium-ion batteries. The comprehensive understanding of the metal-oxide morphology and the local electrochemical properties is essential for figuring out the metal-oxide coating effect. In this study, scanning electrochemical cell microscopy (SECCM) is used to analyze the surface morphology with high spatial resolution, together with the local electrochemical properties.

Lithium-ion batteries (LIBs) are employed in various applications including power sources for mobile devices and electric vehicles.[1] To extend their application range, it is necessary to improve their energy density, rate performance, cycle durability and safety. It is recognized that the cycle durability of LIBs depends on side reactions occurring at the electrode/electrolyte interface.[2] The significance of deterioration at the positive-electrode/electrolyte interface was demonstrated in recent years.[3-5] To improve the durability of LIBs, cathode surface coating with metal oxide, e.g. Al_2O_3, MgO, and ZrO_2, has been studied and validated.[6-9] Various mechanisms for this durability improvement have been suggested, including 1) suppressing volume expansion and contraction of the active materials,[10] 2) inhibiting a side reaction at the interface by surface area reduction[11] and 3) forming a Li-ion conductive surface layer.[12] However, the intrinsic mechanism of the metal-oxide coating effect remains unclear.

To understand the metal oxide coating effect on battery performance, the following two techniques are required: 1) constructing a flat thin-film electrode surface to realize a well-defined interface and 2) analyzing the electrode/electrolyte interface reaction with nanoscale resolution. We previously studied flat $LiCoO_2$ thin-film electrodes using *in situ* surface-sensitive X-ray absorption spectroscopy (XAS) and reported that Co reduction at the $LiCoO_2$ surface resulting from electrolyte contact caused the initial degradation.[13, 14] We also showed that the ZrO_2 layer successfully prevented physical contact between $LiCoO_2$ and the electrolyte. And it confirmed that a thicker ZrO_2 layer (above 2 nm) increased the diffusion resistance of the lithium ions in the ZrO_2 layer.[15] However, since XAS lacks in-plane resolution and provides only averaged information, it is impossible to analyze the ZrO_2 morphology in detail. Recently, Taguchi et al. investigated a thin Li-Zr-layer (ca. 2 nm) on a $LiCoO_2$ composite electrode by transmission electron microscopy (TEM). They suggested that this thin layer could improve the durability.[16] However, it is difficult to analyze the electrochemical properties using TEM. To evaluate the intrinsic mechanism of the metal oxide coating effect, it is necessary to develop a novel *in-situ* method that can analyze the surface morphology with high spatial resolution and simultaneously determine the local electrochemical properties.

Scanning electrochemical microscopy (SECM) is a powerful technique for linking the surface morphology of a sample to its electrochemical properties.[17-20] For the battery materials, the SECM feedback mode is effective in monitoring solid electrolyte interphase formation.[21-24] To directly and quantitatively investigate spatially resolved ionic processes, mercury-capped platinum ultramicroelectrodes were developed and employed for Li^+ imaging based on Li stripping.[25] However, it is difficult to visualize the Li^+ flux in battery materials at the sub-micrometer scale by SECM. Scanning electrochemical cell microscopy (SECCM), which uses a nanopipette as a probe and forms a local electrochemical cell, is effective in characterizing surface reactivity.[26-29] We recently applied SECCM for visualization of electrochemical activities on a lithium-ion battery cathode material at sub-micrometer resolution.[30] The SECCM was applied to collect or provide Li in specified area confined by the nanopipette. Further, it collection visualized the electrochemical properties by scanning the nanopipette as an image. There are some strong advantages in SECCM for battery material research such as its high spatial resolution, small capacitive current, and isolated electrochemical cell.

In this report, we applied SECCM to characterize a ZrO_2-coated $LiCoO_2$ thin-film electrode prepared by pulsed laser deposition. Local cyclic voltammetry (CV) and galvanostatic charge/discharge were performed to characterize the cycle durability and rate performance of ZrO_2-coated $LiCoO_2$ thin-film electrodes and to reveal the relationship between the ZrO_2 morphology and thickness.

Figure 1(a) and (b) show typical cross-sectional STEM images and EDX elemental maps for the $LiCoO_2$ films coated by ZrO_2 for 30 s (Figure 1(a)) and 180 s (Figure 1(b)). The Zr signal was

[a] *Graduate School of Environmental Studies, Tohoku University, 6-6-11-604, Aramaki Aoba, Aoba-ku, Sendai 980-8579, Japan*
[b] *Nano Life Science Institute (WPI-NanoLSI), Kanazawa University, Kakuma-machi, Kanazawa 920-1192, Japan*
[c] *Precursory Research for Embryonic Science and Technology (PRESTO), Japan Science and Technology Agency (JST), Saitama 332-0012, Japan*
[d] *Research&Development Group, Hitachi, Ltd., Hitachi-shi, Ibaraki 319-1292, Japan*
[e] *WPI-Advanced Institute for Materials Research (AIMR), Tohoku University, 2-1-1-509, Katahira, Aoba-ku, Sendai 980-8577, Japan*
[f] *Department of Applied Chemistry, Graduate School of Engineering, Tohoku University, Sendai 980-8579, Japan*
†Electronic Supplementary Information (ESI) available: See DOI: 10.1039/x0xx00000x

distributed at the top of the $LiCoO_2$ films in both cases, although the Zr intensity for the film coated for 180 s was larger than for that coated for 30 s. To estimate the thicknesses of the ZrO_2 layers coated for 30 and 180 s, EDX line profiles of Zr, Co, and O signals were evaluated for four areas for each sample. Corresponding EDX line profiles (Zr, Co, and O) at the lines shown in the STEM images are displayed at the bottom of Figure 1. The thickness of the ZrO_2 layer coated for 30 s was inhomogeneous; that is, a 2 nm thin area (line A-B) coexisted with a 5 nm thick area (not shown). Conversely, the ZrO_2 layer coated for 180 s was homogeneous with a thickness of 5 nm (line C-D). These results indicated that the morphology of the ZrO_2-coated layer varied with the preparation period.

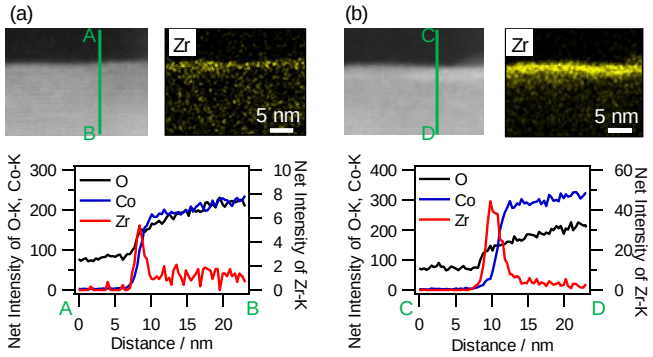

Figure 1. Cross-sectional STEM images; Zr EDX maps (Intensity of Zr-K edge EDX signal) of $LiCoO_2$ thin films ZrO_2-coated for (a) 30 s and (b) 180 s. Corresponding EDX (Zr-K, Co-K and O-K edge) line profiles at lines A-B and C-D are displayed at the bottom.

To reveal the relationship between the morphology of the ZrO_2-coated layer and charge/discharge property, a Li^+ deintercalation current was imaged on $LiCoO_2$ electrodes that were uncoated, or coated by ZrO_2 for 30 and 180 s, using SECCM. In this experiment, the applied voltage was 0.93 V vs. Ag/AgCl to detect Li^+ deintercalation currents, which were binarized with a threshold value of 120 pA. The SECCM current images are shown in Figure 2, together with their histograms. The $LiCoO_2$ electrodes that were uncoated and coated by ZrO_2 for 180 s showed relatively homogeneous high and low current responses, respectively. (Figure 2a, c). Conversely, island-like inhomogeneous current responses are observed for the $LiCoO_2$ electrode coated by ZrO_2 for 30 s (Figure 2b).

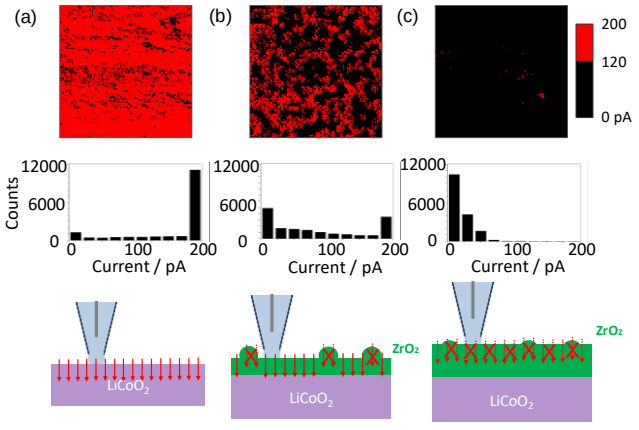

Figure 2. SECCM current and binarization images and histograms for (a) $LiCoO_2$ thin-film electrode, and $LiCoO_2$ thin-film electrodes coated by ZrO_2 for (b) 30 s and (c) 180 s. Threshold current was set to 120 pA. Scan sizes were 5 × 5 μm^2.

The island-like inhomogeneous current response indicates a surface reactivity difference. In the past paper, we imaged a $LiCoO_2$ electrode surface coated by ZrO_2 for 30 s using AFM and visualized similar island-like structure.[15] Also, the STEM images support the SECCM data as an inhomogeneous ZrO_2 thickness (Figure 1a). These results suggest that a 2–5 nm thick metal oxide layer is critical for surface reactivity. To characterize the reactivity difference, we performed local CV at different current response points of the SECCM current image for the $LiCoO_2$ electrode coated by ZrO_2 for 30 s (Figure 3a). We navigated the nanopipette to a selected point in the SECCM image using the self-designed XY position control program. Figure 3c1 and c2 show localized CV measurements at locations corresponding to the high (blue arrow) and low current (red arrow) points in Figure 3a. The CVs at high (left) and low current (right) points resemble those obtained at the randomly selected measurement area on the $LiCoO_2$ electrode coated by ZrO_2 for 30 s (Figure S1c). We also recorded CVs on $LiCoO_2$ electrodes that were uncoated and coated by ZrO_2 for 180 s. From the CV data obtained, it was observed increasing peak separation with ZrO_2-coating (Figure S1a, b). These results indicate that the current response difference is due to the ZrO_2 thickness.

SECCM is also able to visualize the local galvanostatic charge/discharge property. Localized discharge (−20.0 pA for 600 ms, total charge 3 fC) was conducted on a localized area of the $LiCoO_2$ electrode coated by ZrO_2 for 30 s by SECCM, and the potential change during the discharge was monitored at each measurement point (10 ms time resolution, supporting movie 1) to visualize the potential change in the whole scanning area. The scanning size and pixels were set at 4 × 4 μm^2 and 128 × 128, respectively. The 20 pA discharging corresponds to a rate of 10 C, calculated from the CV results. When the nanopipette was just in contact with the surface (0 ms), the potential image appeared homogeneous. However, the potential image observed after 600 ms appeared inhomogeneous (Figure 3b), which was consistent with the inhomogeneous current response shown in Figure 3a. Figure 3d shows potential-time curves for the thin and thick ZrO_2-coated regions. The potential is stable for the thin ZrO_2-coated region, while it is unstable and continues to decrease for the thick ZrO_2-coated region because of the IR-drop due to the ZrO_2 thickness. This result indicates that the thick ZrO_2-coated region degrades the rate performance.

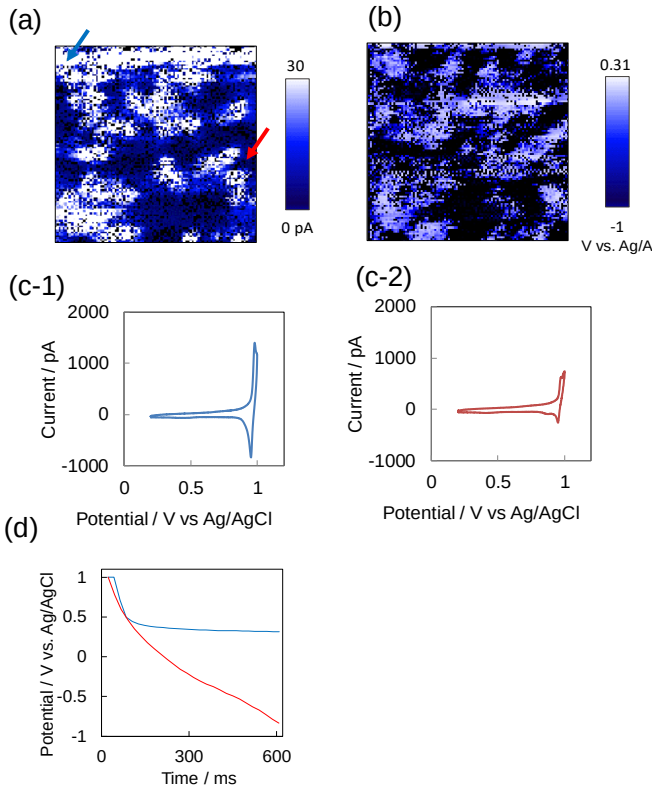

Figure 3. SECCM (a) current and (b) potential images with $LiCoO_2$ thin-film electrodes coated byZrO_2 for 30 s. Scan sizes were 4 × 4 μm^2. The discharge current was 20 pA, and the potential change was monitored for 600 ms. (c) Local CVs and (d) discharge properties at blue and red points of Figure 3(a).

The local cycle durability was investigated by positioning the nanopipette at low and high current response areas of the SECCM image based on deintercalation currents at the $LiCoO_2$ electrode coated by ZrO_2 for 30 s (Figure 4). CVs were continuously recorded for 15 cycles at 100 mV/s to monitor the deterioration process. The CVs show slight changes in the deintercalation/intercalation currents during the continuous cycle (Figure 4b). Figure 4c shows plots of the normalized current response for the reduction peak (intercalation) using the peak current at the second intercalation as a reference. The charge capacity at the thin (blue) and thick (red) ZrO_2-coated areas after 15 cycles remained at 57% and 80%, respectively. This result indicates that ZrO_2-coating is effective in improving the cycle durability of LIBs. The local cycle durability can be rapidly determined using SECCM, as this technique allows CV measurements with high scan rates due to the minimal capacitive current derived from the small electrochemical cell size.

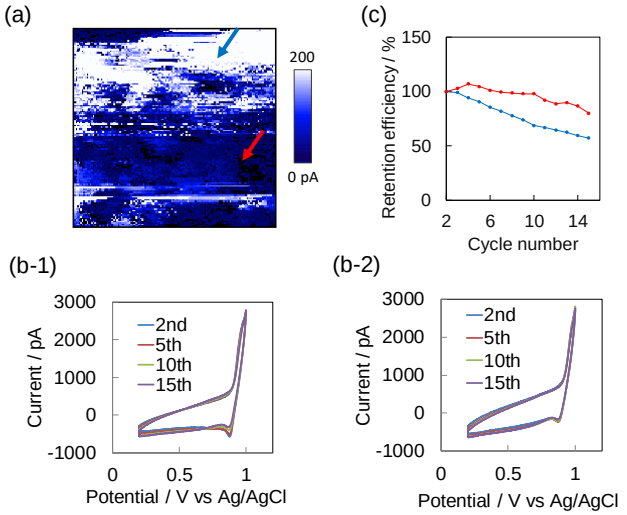

Figure 4. (a) SECCM current image of $LiCoO_2$ thin-film electrode coated by ZrO_2 for 30 s. The scan size was 2 × 2 μm^2. (b) Local CVs and (c) cycle stability characterization using SECCM at the positions of the blue and red arrows in the SECCM image. The scan rate was 100 mV/s.

The above findings confirm that SECCM is effective for characterizing inhomogeneous current distributions at the sub-micrometer scale and for visualizing the ZrO_2 morphology and electrochemical properties at the surface. SECCM is also useful for evaluating the local cycle durability, which is normally buried within the averaged information. The information obtained from SECCM measurements will be used to optimize the balance between cycle stability and rate characteristics by applying a nanoscale coating of metal oxide to the cathode materials of Li-ion batteries.

SECCM is effective in visualizing the morphology and electrochemical properties of ZrO_2-coated $LiCoO_2$ at sub-micrometer resolution. SECCM current imaging visualized an inhomogeneous island-like response distribution for the $LiCoO_2$ coated by ZrO_2 for 30 s. The low and high current response regions correspond to areas with thin and thick ZrO_2-coating, respectively. Localized CV demonstrated that ZrO_2-coating improved the cycle durability at the expense of the reaction rate. Charge/discharge imaging revealed the rate performance inhomogeneity. The present system can be applied widely to nanometer scale characterization of other battery materials.

The authors acknowledge support for this work from Development of Systems and Technology for Advanced Measurement and Analysis from AMED (The Japan Agency for Medical Research and Development)-SENTAN, and ALCA and PRESTO(JPMJPR18T8) from the Japan Science and Technology Agency (JST), a Grant-in-Aid for Scientific Research (A) (16H02280), a Grant-in-Aid for Scientific Research (B) (15H03542), a Grant-in-Aid for Young Scientists (A) (15H05422 and 16H06042), a Grant-in-Aid for Exploratory Research (15K13263), and Grant-in-Aid for Scientific Research on Innovative Areas (16H00885) from the Japan Society for the

Promotion of Science (JSPS) and the Nakatani Foundation, the Asahi Glass Foundation, and Murata Science Foundation.

Conflicts of interest

There are no conflicts to declare.

References

1. M. Armand and J. M. Tarascon, *Nature*, 2008, **451**, 652-657.
2. D. Aurbach, B. Markovsky, G. Salitra, E. Markevich, Y. Talyossef, M. Koltypin, L. Nazar, B. Ellis and D. Kovacheva, *J. Power Sources*, 2007, **165**, 491-499.
3. D. Aurbach, K. Gamolsky, B. Markovsky, G. Salitra, Y. Gofer, U. Heider, R. Oesten and M. Schmidt, *J. Electrochem. Soc.*, 2000, **147**, 1322-1331.
4. D. Aurbach, B. Markovsky, A. Rodkin, E. Levi, Y. S. Cohen, H. J. Kim and M. Schmidt, *Electrochim. Acta*, 2002, **47**, 4291-4306.
5. K. Edstrom, T. Gustafsson and J. O. Thomas, *Electrochim. Acta*, 2004, **50**, 397-403.
6. Z. H. Chen, Y. Qin, K. Amine and Y. K. Sun, *J. Mater. Chem.*, 2010, **20**, 7606-7612.
7. K. T. Lee, S. Jeong and J. Cho, *Acc. Chem. Res.*, 2013, **46**, 1161-1170.
8. C. Li, H. P. Zhang, L. J. Fu, H. Liu, Y. P. Wu, E. Ram, R. Holze and H. Q. Wu, *Electrochim. Acta*, 2006, **51**, 3872-3883.
9. X. B. Meng, X. Q. Yang and X. L. Sun, *Adv. Mater.*, 2012, **24**, 3589-3615.
10. J. Cho, Y. J. Kim, T. J. Kim and B. Park, *Angew. Chem. Int. Ed.*, 2001, **40**, 3367-+.
11. Z. H. Chen and J. R. Dahn, *Electrochem Solid St*, 2002, **5**, A213-A216.
12. M. M. Thackeray, C. S. Johnson, J. S. Kim, K. C. Lauzze, J. T. Vaughey, N. Dietz, D. Abraham, S. A. Hackney, W. Zeltner and M. A. Anderson, *Electrochem. Commun.*, 2003, **5**, 752-758.
13. D. Takamatsu, T. Nakatsutsumi, S. Mori, Y. Orikasa, M. Mogi, H. Yamashige, K. Sato, T. Fujimoto, Y. Takanashi, H. Murayama, M. Oishi, H. Tanida, T. Uruga, H. Arai, Y. Uchimoto and Z. Ogumi, *J. Phys. Chem. Lett.*, 2011, **2**, 2511-2514.
14. D. Takamatsu, Y. Koyama, Y. Orikasa, S. Mori, T. Nakatsutsumi, T. Hirano, H. Tanida, H. Arai, Y. Uchimoto and Z. Ogumi, *Angew. Chem. Int. Ed.*, 2012, **51**, 11597-11601.
15. D. Takamatsu, S. Mori, Y. Orikasa, T. Nakatsutsumi, Y. Koyama, H. Tanida, H. Arai, Y. Uchimoto and Z. Ogumi, *J. Electrochem. Soc.*, 2013, **160**, A3054-A3060.
16. N. Taguchi, H. Sakaebe, T. Akita, K. Tatsumi and Z. Ogumi, *J. Electrochem. Soc.*, 2014, **161**, A1521-A1526.
17. E. Ventosa and W. Schuhmann, *PCCP*, 2015, **17**, 28441-28450.
18.D. Polcari, P. Dauphin-Ducharme and J. Mauzeroll, *Chem. Rev.*, 2016, **116**, 13234-13278.
19. Y. Takahashi, A. Kumatani, H. Shiku and T. Matsue, *Anal. Chem.*, 2017, **89**, 342-357.
20. L. Danis, S. M. Gateman, C. Kuss, S. B. Schougaard and J. Mauzeroll, *Chemelectrochem*, 2017, **4**, 6-19.
21. G. Zampardi, E. Ventosa, F. La Mantia and W. Schuhmann, *Chem. Commun.*, 2013, **49**, 9347-9349.
22. E. Ventosa, G. Zampardi, C. Flox, F. La Mantia, W. Schuhmann and J. R. Morante, *Chem. Commun.*, 2015, **51**, 14973-14976.
23. G. Zampardi, F. La Mantia and W. Schuhmann, *Rsc Adv*, 2015, **5**, 31166-31171.
24. J. S. Hui, M. Burgess, J. R. Zhang and J. Rodriguez-Lopez, *Acs Nano*, 2016, **10**, 4248-4257.
25. Z. J. Barton and J. Rodriguez-Lopez, *Anal. Chem.*, 2014, **86**, 10660-10667.
26. A. G. Guell, A. S. Cuharuc, Y. R. Kim, G. H. Zhang, S. Y. Tan, N. Ebejer and P. R. Unwin, *Acs Nano*, 2015, **9**, 3558-3571.
27. B. D. B. Aaronson, C. H. Chen, H. J. Li, M. T. M. Koper, S. C. S. Lai and P. R. Unwin, *J Am Chem Soc*, 2013, **135**, 3873-3880.
28. A. G. Guell, N. Ebejer, M. E. Snowden, J. V. Macpherson and P. R. Unwin, *J. Am. Chem. Soc.*, 2012, **134**, 7258-7261.
29. M. E. Snowden, M. Dayeh, N. A. Payne, S. Gervais, J. Mauzeroll and S. B. Schougaard, *J. Power Sources*, 2016, **325**, 682-689.
30. Y. Takahashi, A. Kumatani, H. Munakata, H. Inomata, K. Ito, K. Ino, H. Shiku, P. R. Unwin, Y. E. Korchev, K. Kanamura and T. Matsue, *Nat Commun*, 2014, **5**, 5450.

